James P. Denier · Matthew D. Finn
Editors

# Mechanics Down Under

Proceedings of the 22nd International Congress of Theoretical and Applied Mechanics, held in Adelaide, Australia, 24–29 August 2008

Springer

*Editors*

Prof. James P. Denier
Department of Engineering Science
The University of Auckland
Auckland
New Zealand

Dr. Matthew D. Finn
School of Mathematical Sciences
The University of Adelaide
South Australia
Australia

Additional material to this book can be downloaded from http://extras.springer.com

ISBN 978-94-007-5967-1 e-ISBN 978-94-007-5968-8
DOI 10.1007/978-94-007-5968-8
Springer Dordrecht Heidelberg New York London

Library of Congress Control Number: 2012953386



Printed on acid-free paper

Springer is part of Springer Science+Business Media (www.springer.com)

# Material Instabilities in Elastic and Plastic Solids: The Perturbative Approach

Davide Bigoni

Department of Mechanical and Structural Engineering, University of Trento,
via Mesiano 77, I-38050 Trento, Italy
bigoni@ing.unitn.it

The perturbative approach to material instabilities introduced by Bigoni and Capuani [2],[3] (in which a perturbing agent is superimposed to a uniformly stressed and strained infinite medium) is reviewed and applied to show how randomly-distributed dislocation-like defects can induce strain patterns in ductile metallic materials, prestressed near the border of ellipticity loss. These patterns result to be strongly focussed and organized into shear bands, evidencing a well-defined texture in the material.

## 1 Introduction

A *material instability* is usually identified with a localized loss of homogeneity of deformation occurring in a solid sample subject to a loading path compatible with continued uniform deformation and constrained on the whole boundary to prescribed displacements (or to smooth contact with a rigid wall [14]), Fig. 1. Since the stiff boundary constraint prevents development of 'global' (such as Euler-like buckling) or surface (such as necking) bifurcations, the loss of homogeneity occurring in the sample may be interpreted as a deformation mechanism 'alternative' to the homogeneous one, or, in other words, as a 'localized' bifurcation. Roughly speaking, this bifurcation results from a strongly nonlinear (nominal) stress versus (conventional) strain curve of the type sketched in Fig. 2 (referred to the experiment on drinking straw packaging reported in Fig. 3), exhibiting an initial linear response, followed by a nonlinear range, evidencing a peak and subsequent strain softening.[1]

[1] Note that in experiments of the type shown in Fig. 1, it is difficult to envisage by a purely visual inspection if the localization of deformation occurs just *before or after the peak* (in other words, whether softening is necessary to localization, or softening results from localization), but this is certainly already present during the softening response.

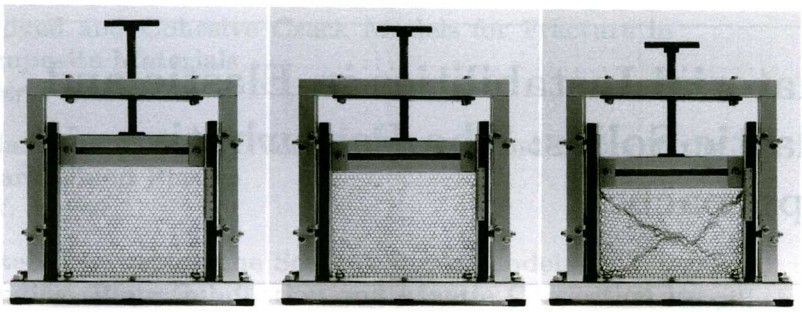

**Fig. 1** Uniaxial deformation of a regular packaging of identical and parallel thin-walled cylinders (drinking straws), constrained within a rigid-wall box. The unloaded configuration is shown left and a configuration where deformation is still homogeneous is shown at the centre. While the strong confinement precludes diffuse bifurcations, strain localization can develop and is visible on the right (experiment inspired from [12] and performed at the University of Trento).

The softening may, as in Fig. 2, terminate at a certain strain level to give rise to a more or less pronounced strain hardening regime.

The strain localization visible in the experiment shown in Fig. 1 is only a 'strong and evident manifestation' that the material traverses an unstable state, beginning at a certain –sufficiently high – strain level, culminating with localization and (as in the case of the drinking straw packaging) continuing with an accumulation of deformation bands (or in other cases with intense deformation and damage within a single deformation band, [8]).

Since the 'standard' approach to material instability is limited to the determination of the *onset* of strain localization (identified with the loss of ellipticity of the incremental governing equations [13]), the unstable state previously traversed by the material is usually left unexplored. However, this state can efficaciously be investigated through the analysis of the material response to a *perturbation* applied at a certain level of deformation. For instance, we can perturb the sample in the experiment shown in Fig. 1, by applying a concentrated force when the deformation is still uniform, but the peak of the curve is approached (Fig. 3). As a result, the deformation induced by the perturbing force becomes highly focussed and localized, which would have not been the case if the perturbation were provided much before the peak of the stress/strain response. This experimental procedure has been rationalized by Bigoni and Capuani [2], who have defined a perturbation in terms of a concentrated force acting in an infinite prestressed continuum. In addition to the concentrated force, different perturbing agents have been envisaged, namely, a fracture, a rigid-thin inclusion, and a pre-existing shear band, so that the perturbative approach has been shown to be 'rich enough' to give evidence to phenomena involving dynamics of shear bands [3], strain pattern emergence for materials in flutter conditions [11], and interactions between shear bands and inclusions [4]–[7].

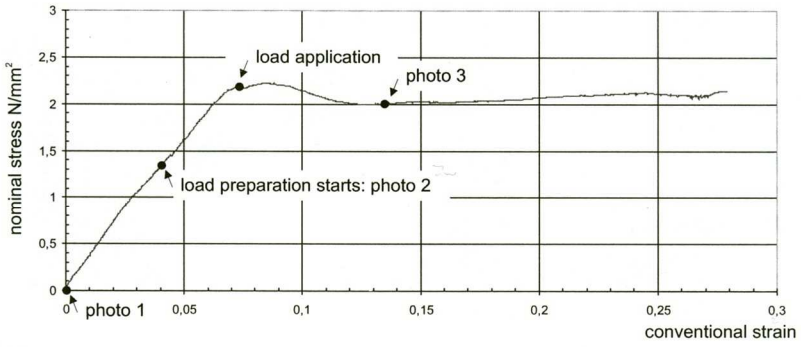


**Fig. 2** Vertical nominal stress versus 'global' uniaxial conventional strain curve for a packaging of regularly disposed drinking straws obtained at a speed of the piston of 5mm/min. Note that, due to the lateral constraint, the state of stress in the test is not uniaxial. The indication of the photos refers to Fig. 3, where the application of a vertical concentrated load is visible. The velocity of the imposed vertical motion of the rigid piston has decreased from 5 mm/min to 1 mm/min when the concentrated load has applied.

We complement the above results in the present article with an analysis of the effects of a random distribution of dislocation-like defects on a prestressed, ductile material, showing that defects induce a well-oriented texture within a material, when prestressed near the elliptic border. To this purpose, we start introducing the infinite-body Green's function set for a prestressed, incompressible material, we continue showing analogies between force and dislocation dipoles (namely, for a special geometrical setting the far fields can be made to coincide for incompressible and isotropic elasticity) and, finally, we present results for random distributions of dipoles, simulating dislocation-like defects.

## 2 Infinite-Body, Quasi-Static Green's Function for an Incompressible, Prestressed Material

Green's functions for anisotropic prestressed materials have been found by Willis [15] and Bigoni and Capuani [2],[3]. We focus attention to two-dimensional Green's functions, considering the case of incompressible, anisotropic prestressed elasticity[2], solved by Bigoni and Capuani [2], whose incremental constitutive equations are written in terms of nominal stress increment $\dot{t}_{ij}$, functions of incremental displacement gradient $v_{i,j}$ and in-plane mean stress $\dot{p}$

[2] The case of compressible materials, including the loading branch of a generic elastoplastic constitutive operator, has been treated by Bertoldi et al. [1] for the quasi-static case and Piccoloraz et al. [11] for the dynamic case.

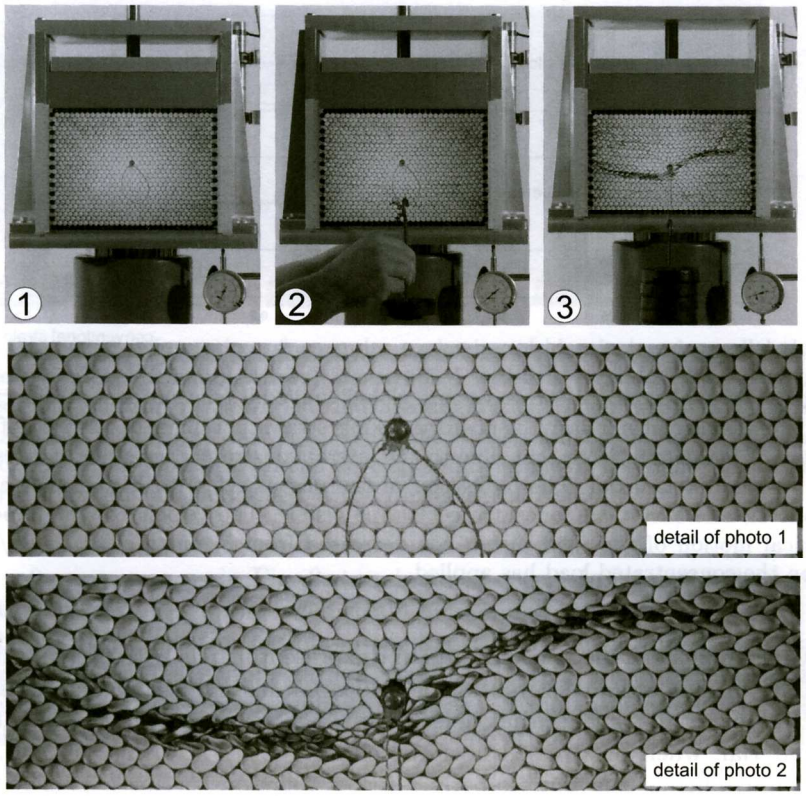


**Fig. 3** Application of a concentrated load (50 N) during uniaxial deformation of a packaging of regularly disposed drinking straws. Photo 1 has been taken before the test start, while a vertical load has been applied at the instant when photo 2 has been taken. The shear bands emanating from the applied load are visible in photo 3. The two photos reported below are details of photo 1 (unloaded configuration) and 3 (strain localization already developed), where the device used to apply the concentrated load is visible.

$$\begin{aligned} \dot{t}_{11} &= \mu(2\xi - k - \eta)v_{1,1} + \dot{p}, & \dot{t}_{22} &= \mu(2\xi + k - \eta)v_{2,2} + \dot{p}, \\ \dot{t}_{12} &= \mu[(1+k)v_{2,1} + (1-\eta)v_{1,2}], & \dot{t}_{21} &= \mu[(1-\eta)v_{2,1} + (1-k)v_{1,2}], \end{aligned} \tag{1}$$

where the dimensionless parameters

$$\xi = \frac{\mu_*}{\mu}, \quad \eta = \frac{p}{\mu} = \frac{T_1 + T_2}{2\mu}, \quad k = \frac{T_1 - T_2}{2\mu}, \tag{2}$$

are functions of the current principal Cauchy stresses $T_1$, $T_2$ and of two incremental shear moduli, $\mu$ and $\mu_*$.

Equilibrium equations expressed in terms of the stream function,

$$v_1^g = \psi^g_{,2}, \quad v_2^g = -\psi^g_{,1}, \tag{3}$$

can be written including a concentrated force of unit components, $\delta_{ig}\,\delta(\boldsymbol{x})$, as

$$(1+k)\psi^g_{,1111}+2(2\xi-1)\psi^g_{,1122}+(1-k)\psi^g_{,2222}+\frac{\delta_{1g}\delta_{,2}(\boldsymbol{x})-\delta_{2g}\delta_{,1}(\boldsymbol{x})}{\mu}=0. \tag{4}$$

Employing a plane wave expansion of the stream function $\psi^g$, which for a generic function $h$ is written as

$$h(\boldsymbol{x}) = -\frac{1}{4\pi^2}\oint_{|\boldsymbol{n}|=1}\tilde{h}(\boldsymbol{n}\cdot\boldsymbol{x})\mathrm{d}\boldsymbol{n}, \tag{5}$$

(where $\boldsymbol{n}$ is the radial unit vector centred at the origin of the position vector $\boldsymbol{x}$) and enjoying the following properties

$$\tilde{\delta}(\boldsymbol{n}\cdot\boldsymbol{x}) = \frac{1}{(\boldsymbol{n}\cdot\boldsymbol{x})^2}, \quad \nabla_{\boldsymbol{x}}\tilde{h}(\boldsymbol{n}\cdot\boldsymbol{x}) = \tilde{h}'(\boldsymbol{n}\cdot\boldsymbol{x})\,\boldsymbol{n}, \tag{6}$$

(where the prime denotes differentiation with respect to the argument $\boldsymbol{n}\cdot\boldsymbol{x}$), equation (4) becomes the ordinary differential equation

$$L(\boldsymbol{n})\left(\tilde{\psi}^g\right)'''' = 2\frac{\delta_{1g}n_2-\delta_{2g}n_1}{(\boldsymbol{n}\cdot\boldsymbol{x})^3}, \tag{7}$$

where the (strictly positive in the elliptic regime) function $L(\boldsymbol{n})$ has been introduced

$$L(\boldsymbol{n}) = \mu\, n_2^4\,(1+k)\left(\frac{n_1^2}{n_2^2}-\frac{1-k}{1+k}\Omega_2^2\right)\left(\frac{n_1^2}{n_2^2}-\frac{1-k}{1+k}\Omega_1^2\right) > 0, \tag{8}$$

in which $\Omega_i^2$ are the squares of the roots of the homogeneous associated characteristic equation to (4).

A straightforward integration of (7) yields

$$\tilde{\psi}^g = \frac{\delta_{1g}n_2-\delta_{2g}n_1}{L(\boldsymbol{n})}(\boldsymbol{n}\cdot\boldsymbol{x})\left(\log|\boldsymbol{n}\cdot\hat{\boldsymbol{x}}|-1\right), \tag{9}$$

which, antitransformed, leads to the Green's stream function

$$\begin{aligned}\psi^g = -\frac{r}{2\pi^2\mu(1+k)}\Bigg[&(\log\hat{r}-1)\int_0^{\pi}\frac{\sin[\alpha+\theta+(1-g)\pi/2]\cos\alpha}{\Lambda(\alpha+\theta)}\,\mathrm{d}\alpha\\ &+\int_0^{\pi/2}\frac{\sin[\alpha+\theta+(1-g)\pi/2]\cos\alpha\log(\cos\alpha)}{\Lambda(\alpha+\theta)}\,\mathrm{d}\alpha\\ &-\int_0^{\pi/2}\frac{\cos[\alpha+\theta+(1-g)\pi/2]\sin\alpha\log(\sin\alpha)}{\Lambda(\alpha+\theta+\pi/2)}\,\mathrm{d}\alpha\Bigg],\end{aligned} \tag{10}$$

where

$$\Lambda(\alpha) = \sin^4\alpha\,\left(\cot^2\alpha - \gamma_1\right)\left(\cot^2\alpha - \gamma_2\right) > 0. \tag{11}$$

Employing now the definition of stream function (3) yields the Green's function for incremental displacements

$$v_j^g = \frac{1}{2\pi^2\mu(1+k)}\left\{\frac{\pi\,\delta_{jg}\,\log r}{\left[(2-j)\,\gamma_2 + 1 - j\right]\sqrt{-\gamma_1} + \left[(2-j)\,\gamma_1 + 1 - j\right]\sqrt{-\gamma_2}}\right.$$
$$\left. - \int_0^{\frac{\pi}{2}} \left[K_j^g(\alpha+\theta) + (3-2j)\,(3-2g)\,K_j^g(\alpha-\theta)\right]\log\left(\cos\alpha\right)\mathrm{d}\alpha\right\}, \tag{12}$$

where

$$K_j^g(\alpha) = \frac{\sin\left[\alpha + (j-1)\frac{\pi}{2}\right]\sin\left[\alpha + (g-1)\frac{\pi}{2}\right]}{\Lambda\left(\alpha\right)}, \tag{13}$$

The solution for the Green's function set for an incompressible material is not yet complete, since the knowledge of the velocity gradient does not allow determination of the Green's function for in-plane incremental mean stress $\dot{p}^g$. Therefore, we consider the rate equilibrium equations written for the Green's function set $\{v_i^g, \dot{p}^g\}$

$$\begin{aligned} \dot{p}^g_{,1} - \mu\,k v^g_{1,11} &= \mu[(1-2\xi)v^g_{1,11} - (1-k)v^g_{1,22}] - \delta_{1g}\delta(\boldsymbol{x}), \\ \dot{p}^g_{,2} - \mu\,k v^g_{1,12} &= \mu[(1-2\xi)v^g_{2,22} - (1+k)v^g_{2,11}] - \delta_{2g}\delta(\boldsymbol{x}). \end{aligned} \tag{14}$$

Introducing now the in-plane mean nominal stress

$$\dot{\pi} = \frac{\dot{t}_{11} + \dot{t}_{22}}{2} = \dot{p} - \mu\,k v_{1,1}, \tag{15}$$

differentiating eqn. (14a) with respect to $x_1$, eqn. (14b) with respect to $x_2$ and summing the resulting equations yields

$$\begin{aligned} \frac{\dot{\pi}_{,11} + \dot{\pi}_{,22}}{\mu} &= 2(1-\xi)\left(v_{1,111} + v_{2,222}\right) \\ &\quad + k\left(v_{1,111} - v_{2,222}\right) - \frac{\delta_{1g}\delta_{,1}(\boldsymbol{x}) + \delta_{2g}\delta_{,2}(\boldsymbol{x})}{\mu}, \end{aligned} \tag{16}$$

which in the transformed domain becomes the ordinary differential equation

$$\begin{aligned} \frac{(\tilde{\pi}^g)''}{\mu} &= 2(1-\xi)\left[n_1^3\,(\tilde{v}_1^g)''' + n_2^3\,(\tilde{v}_2^g)'''\right] \\ &\quad + k\left[n_1^3\,(\tilde{v}_1^g)''' - n_2^3\,(\tilde{v}_2^g)'''\right] + 2\frac{n_1\delta_{1g} + n_2\delta_{2g}}{\mu(\boldsymbol{n}\cdot\boldsymbol{x})^3}. \end{aligned} \tag{17}$$

Since $\tilde{v}_i^g$ and its derivatives are known from differentiation of equation (9), (17) can be integrated and antitransformed to give the Green's function for the in-plane mean nominal stress increment

$$\dot{\pi}^g = -\frac{1}{2\pi r}\left\{\cos\left[\theta-(g-1)\frac{\pi}{2}\right]+\frac{1}{\pi(1+k)}\int_0^\pi \frac{\tilde{K}_g(\alpha+\theta)}{\cos\alpha}\mathrm{d}\alpha\right\}, \tag{18}$$

where

$$\tilde{K}_g(\alpha) = K_g^g(\alpha)\left[2\left(\frac{\mu_*}{\mu}-1\right)\left(2\cos^2\alpha-1\right)-k\right]\cos\left[\alpha+\delta_{2g}\frac{\pi}{2}\right], \tag{19}$$

completing the infinite-body Green's function set. In particular, application of the constitutive equations (1)-(2) to the Green's velocity gradient and adding the Green's in-plane mean nominal stress (18) yields the Green's function for the incremental nominal stress

$$\begin{aligned} &\dot{t}_{11}^g = (2\mu_*-p)\,v_{1,1}^g+\dot{\pi}^g, && \dot{t}_{22}^g = (2\mu_*-p)\,v_{2,2}^g+\dot{\pi}^g,\\ &\dot{t}_{12}^g = (\mu-p)\,v_{1,2}^g+\left(\mu+\frac{\sigma}{2}\right)v_{2,1}^g, && \dot{t}_{21}^g = (\mu-p)\,v_{2,1}^g+\left(\mu-\frac{\sigma}{2}\right)v_{1,2}^g. \end{aligned} \tag{20}$$

## 3 Dipoles in an Infinite Medium

Superimposing the effects, the Green's function (12) can be used to investigate the response of a homogeneously prestressed infinite medium perturbed by a quasi-statically applied dipole (two equal and opposite concentrated forces placed at a distance, say, $2a$). The analysis of the resulting incremental displacement maps at different 'distances' from the border of ellipticity provides information on the behaviour of the material near a material instability [2].

An example is reported in Fig. 4, referred (as all other examples addressed in the following) to a material following the $J_2$–deformation theory of plasticity, namely, a nonlinear elastic law corresponding to the loading branch of von Mises plasticity, so that unloading is *a-priori* excluded [10]. The figure clearly indicates that, *while at null prestress the incremental deformation field does not evidence a particular structure* (Fig. 4 on the left), *a shear band pattern emerges as the response to the dipole perturbation at a prestress level near the boundary of (but still inside) ellipticity* (Fig. 4 on the right).

A quasi-static dipole represents the simplest 'zero-resultant-force' perturbation, so that many other possible perturbations can be invented to capture 'particular' effects. For instance, Bigoni and Capuani [3] have employed a time-harmonic pulsating dipole to obtain incremental displacements maps similar to that reported in Fig. 5 (referred to the same material considered in Fig. 4) and showing an interesting wave focussing, an effect which becomes critical to detect the so-called 'flutter instability' [11].

While other perturbing agents will be discussed later, our interest now is to analyze the effect of a random distribution of randomly oriented dipoles, a situation which may represent the presence of defects in a material and, in

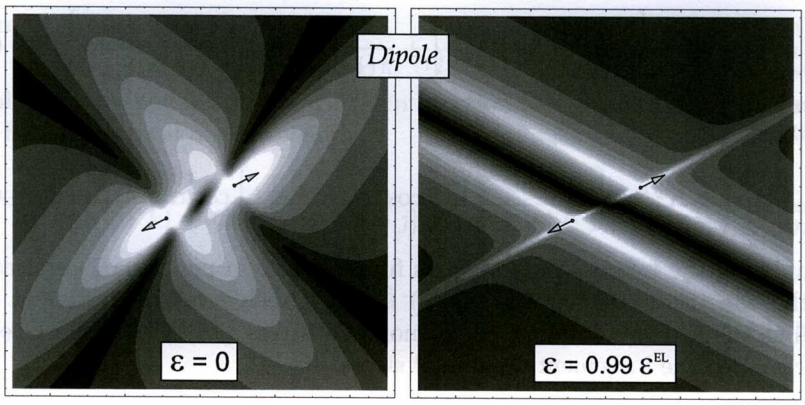


**Fig. 4** Incremental displacement map resulting as the response of an unloaded (left) material and the same material prestrained close to the elliptic boundary (right) to a perturbing dipole (inclined at an angle of 27.367° with respect to the horizontal axis, corresponding to the shear band inclination at the elliptic boundary). A ductile metallic material (modelld through the $J_2$-deformation theory of plasticity) has been considered with an hardening exponent $N = 0.4$. Parameter $\varepsilon$ denotes the logarithmic prestrain and $\varepsilon^{EL}$ the value corresponding to ellipticity loss.

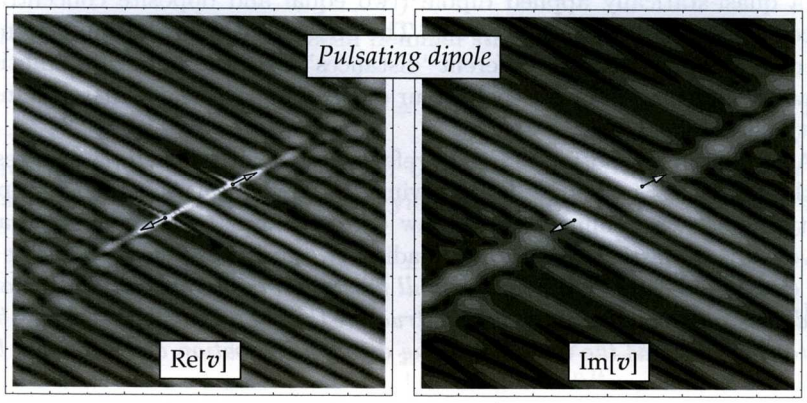


**Fig. 5** A time-harmonic pulsating dipole is perturbing a ductile metallic ($J_2$-deformation theory) material near the elliptic border ($\varepsilon = 0.99\varepsilon^{EL}$), as in Fig. 4 on the right. Here the solution is the sum of a real (left) and imaginary (right) part. Note the focussing of the waves revealing formation of a complex shear band pattern.

particular, these defects can be representative of a dislocation distribution.[3] In fact, there are analogies between the solutions of a concentrated force and a dislocation in an elastic continuum and, we show below that *when the prestress is absent and for isotropic incompressible elasticity, the far-fields induced by a dislocation dipole on a single slip plane and a force dipole inclined at $\pi/4$ with respect to this plane are identical.*

In a $x$–$y$ reference system, the in-plane stress field produced by *a single straight edge dislocation* in a linearly elastic, isotropic medium is [9]

$$\{\sigma_{xx}, \sigma_{yy}, \sigma_{xy}\} = \frac{b\,\mu}{2\pi(1-\nu)\,r^4}\left\{-y\left(3x^2+y^2\right),\ y\left(x^2-y^2\right),\ x\left(x^2-y^2\right)\right\}, \tag{21}$$

where $b$ is the Burgers vector and $\mu$ and $\nu$ are the elastic shear modulus and the Poisson's ratio. The corresponding strain field follows from eqn. (21) in the form

$$\{\epsilon_{xx}, \epsilon_{yy}, \epsilon_{xy}\} = \frac{1}{\bar{E}}\left\{\sigma_{xx} - \bar{\nu}\sigma_{yy},\ \sigma_{yy} - \bar{\nu}\sigma_{xx},\ (1+\bar{\nu})\sigma_{xy}\right\}, \tag{22}$$

where $\bar{E}$ and $\bar{\nu}$ are the modified Young modulus and Poisson's ratio, while the displacement field can be written as

$$\begin{aligned} u_x &= \frac{b}{2\pi}\left[\arctan\frac{y}{x} + \frac{xy}{2(1-\nu)r^2}\right], \\ u_y &= -\frac{b}{8\pi\,(1-\nu)}\left[(1-2\nu)\log r^2 + \frac{x^2-y^2}{r^2}\right]. \end{aligned} \tag{23}$$

A dislocation dipole on a single glide plane consists of two parallel edge dislocations lying in the same slip plane at a distance $2d$ and having opposite sign (see Fig. 6 on the left for a sketch of the distortion induced in a crystal lattice and on the right for its graphical conventional representation). In quasi-static conditions, such a simple dislocation structure is not stable, so that the dislocations, unless pinned, 'attract' each other to reduce their total elastic energy. In this way they move toward each other until they combine and annihilate.

Leaving aside issues on stability, the stress field produced by the dislocation dipole can simply be obtained through superposition of solution (21), which can be used with reference to the local coordinates (Fig. 6 on the right)

$$x_i = x+(-1)^i d, \quad y_i = y, \quad r_i^2 = [x+(-1)^i d]^2+y^2 = r^2+(-1)^i xd+d^2, \tag{24}$$

where $i = 1, 2$.

At a large distance from the dislocation dipole the parameter $d/r$ can be considered small and the stress fields can be expanded into a Taylor series, to obtain the far field approximation

[3] The analogy between dislocation and force dipoles has been suggested to me by Prof. A.B. Movchan (Liverpool University).

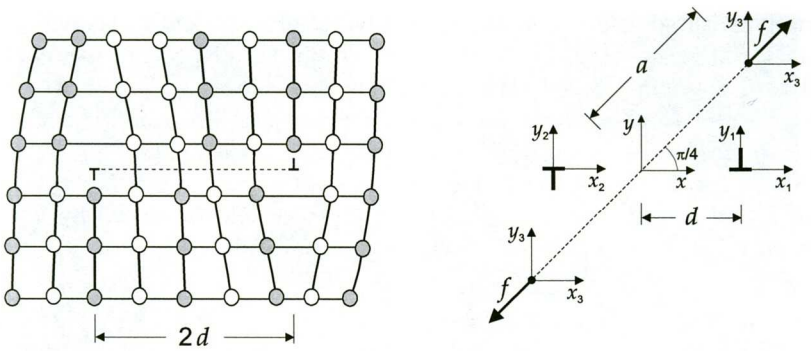


**Fig. 6** Sketch of the lattice distortion induced by a dislocation dipole lying on a single slip plane (left) and its conventional representation (right), together with a force dipole (inclined at $\pi/4$ with respect to $x$–$y$ system). In linear isotropic *incompressible* elasticity, the far-fields induced by the dislocation dipole and by the force dipole are identical.

$$\{\sigma_{xx}, \sigma_{yy}, \sigma_{xy}\} \sim \frac{\mu\, d\, b}{\pi(1-\nu)\, r^6} \left\{2xy\left(r^2-4x^2\right),\ 2xy\left(r^2-4y^2\right),\ r^4-8x^2y^2\right\}, \tag{25}$$

which satisfies equilibrium equations.

The far-field stress field for a force dipole in linear elasticity can be obtained by superimposing the solution (20) in the case of null prestress and isotropy as (for a force centered at the origin of a $x$–$y$ reference system)

$$\left\{\sigma^g_{xx},\, \sigma^g_{yy},\, \sigma^g_{xy}\right\} = -\frac{g}{\pi\, r^4}\left\{x^2,\, y^2,\, xy\right\}, \tag{26}$$

where $g$, either equal to $x$ or $y$, denotes the unit component of the applied force. Expressing (26) in the local coordinate systems shown in Fig. 6 on the right, so that

$$\begin{aligned} x_i &= x + (-1)^i a, \quad y_i = y + (-1)^i a \sin\alpha, \\ r_i^2 &= [x + (-1)^i a\cos\alpha]^2 + [y + (-1)^i a \sin\alpha]^2 \\ &= r^2 + (-1)^i a(x\cos\alpha + y\sin\alpha) + a^2, \end{aligned} \tag{27}$$

where $i = 3, 4$, the dipole solution can be easily obtained. At a large distance from the force dipole, the dimensionless parameter $a/r$ becomes small, so that a Taylor series expansion of the stress fields gives again representation (25) with the correspondence

$$fa = 2db\mu, \tag{28}$$

where $f$ is the modulus of the forces forming the dipole (inclined at $\pi/4$).

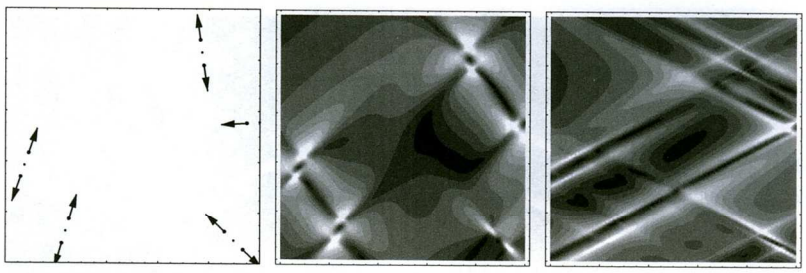

**Fig. 7** Effects of prestrain on a ductile metallic ($J_2$–deformation theory) material (as in Fig. 4), revealed by a perturbation consisting of five randomly placed and oriented dipoles, representing dislocation-like defects (these are shown on the left, where the distance between dipole forces provides the bar scale of the representation). Maps of incremental displacements induced by the dipoles are shown on the centre at null prestrain ($\varepsilon = 0$) and on the right at a prestain near loss of ellipticity ($\varepsilon = 0.99\varepsilon^{EL}$).

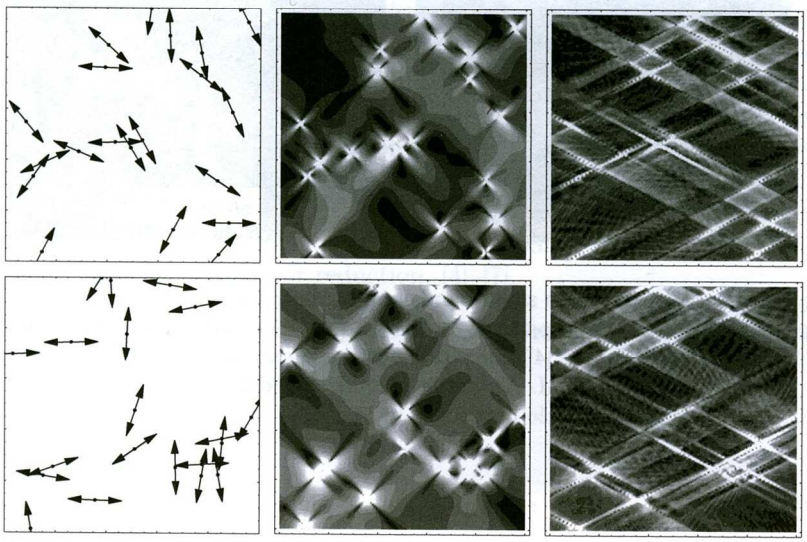

**Fig. 8** As in Fig. 7, but now there are two different random distributions (upper and lower part) of twenty randomly oriented dipoles, representing dislocation-like defects

The effects of prestress have been explored by perturbing a uniform strain field with a random distribution of randomly oriented force dipoles (randomness has been obtained by using the pseudorandom real number generation function available in Mathematica© 5.2). In particular, a square window of material of edge $20a$ ($200a$) has been considered in Fig. 7 (Fig. 8), where $a$ is the half distance between the forces forming the dipole. Inside this window

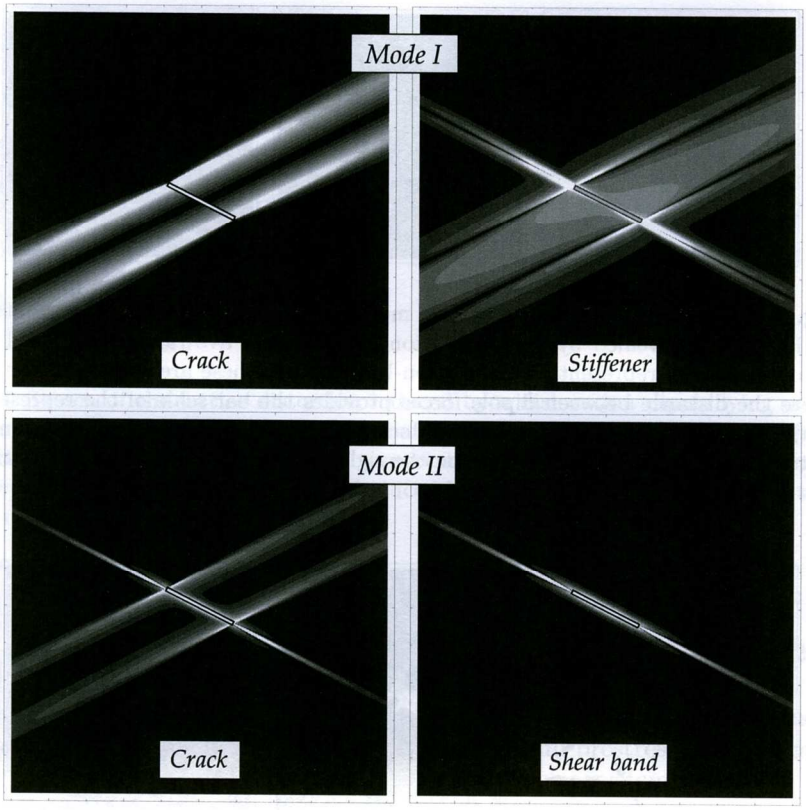


**Fig. 9** Interactions between shear bands and a crack (upper part, left, see [4]), or a thin rigid inclusion (upper part, right, see [5], [6], [7]) –loaded under Mode I–, or a crack (lower part, left, see [4]), or a pre-existing shear band (lower part, right, see [4]) – loaded under Mode II. A ductile metallic ($J_2$–deformation theory) material is considered near the elliptic border, as in Fig. 4.

5 (20) dipoles have been randomly placed in Fig. 7 (Fig. 8), with random inclination of the forces (two random distributions have been reported in Fig. 8). The dipole distributions and inclinations are shown in Figs. 7 and 8 on the left, while the maps of modulus of displacements are shown on the centre for null prestrain ($\varepsilon = 0$, as in Fig. 4 on the left) and on the right for a prestrain near the boundary of loss of ellipticity ($\varepsilon = 0.99\varepsilon^{EL}$, as in Fig. 4 on the right).

The figures reveal that the effect of prestrain consists in *the emerging of a texture with privileged directions, corresponding to the shear band inclinations that can be calculated at the boundary of ellipticity loss.*

## 4 The Perturbative Approach: Conclusions and Perspectives

The conventional approach to material instability is confined to the analysis of failure of ellipticity for a uniformly deformed solid, yielding the threshold of the instability (in terms of a control parameter, for instance, the level of prestress, or the hardening) and the shear band inclinations [13]. Assuming that this conventional analysis can easily be performed and its results are available, the perturbative approach to material instability has been tailored to analyze the unstable state that is traversed by the material *before* ellipticity loss. In this way, features of this unstable state, otherwise remaining simply undetected, can be investigated. As an example, effects of a random distribution of dislocation-like defects acting in a ductile material prestressed near the elliptic boundary have been analyzed in the present article (Figs. 7 and 8). It has been found that these defects trigger incremental deformation patterns showing a well-defined texture, organized along shear bands. The obtained results fit coherently with previous findings concerning: (i) dynamical effects near the border of ellipticity (Fig. 5, see also [3]), or near the so-called 'flutter instability' [11]; (ii) interactions of a shear band with a thin rigid inclusion, or with a crack, or with a pre-existing shear band (see Fig. 9 containing a collection of results than can be compared to each other and to the previous figures). In all these problems, where defects incrementally perturb a prestressed solid, the resulting complex stress states (involving singularities and high stress concentrations) can be detailed through analytical solutions and employed to study incremental energy release rate and the associated tendency to defect growth or reduction, [4]–[7].

**Acknowledgments.** Financial support of MIUR–Prin 2007 (2007YZ3B24_002) is gratefully acknowledged.

## References

1. Bertoldi, K., Brun, M., Bigoni, D.: Int. J. Numer. Meth. Eng. 64, 877–906 (2005)
2. Bigoni, D., Capuani, D.: J. Mech. Phys. Solids 50, 471–500 (2002)
3. Bigoni, D., Capuani, D.: J. Mech. Phys. Solids 53, 1163–1187 (2005)
4. Bigoni, D., Dal Corso, F.: Proc. R Soc. Lond. A 464, 2365–2390 (2008)
5. Bigoni, D., Dal Corso, F., Gei, M.: J. Mech. Phys. Solids 56, 839–857 (2008)
6. Dal Corso, F., Bigoni, D.: Proc. R Soc. Lond. A (2008) (in press)
7. Dal Corso, F., Bigoni, D., Gei, M.: J. Mech. Phys. Solids 56, 815–838 (2008)
8. Gajo, A., Bigoni, D., Muir Wood, D.: J. Mech. Phys. Solids 52, 2683–2724 (2004)
9. Hirth, J.P., Lothe, J.: Theory of dislocations. J. Wiley & Sons, New York (1968)
10. Hutchinson, J.W., Neale, K.W.: Finite strain J2-deformation theory. In: Carlson, D.E., Shield, R.T. (eds.) Proc. IUTAM Symp. on Finite Elasticity, Martinus Nijhoff, The Hague (1979)

11. Piccolroaz, A., Bigoni, D., Willis, J.R.: J. Mech. Phys. Solids 54, 2391–2417 (2006)
12. Poirier, C., Ammi, M., Bideau, D., Troadec, J.P.: Phys. Rev. Lett. 68, 216–219 (1992)
13. Rice, J.R.: The localization of plastic deformation. In: Koiter, W.T. (ed.) Theoretical and Applied Mechanics, North-Holland, Amsterdam (1977)
14. Ryzhak, E.I.: J. Mech. Phys. Solids 41, 1345–1356 (1993)
15. Willis, J.R.: Inclusions and cracks in constrained anisotropic media. In: Wu, J.J., Ting, T.C.T., Barnett, D.M. (eds.) Modern Theory of Anisotropic Elasticity and Applications. SIAM, Philadelphia (1991)